General Disclaimer

One or more of the Following Statements may affect this Document

- This document has been reproduced from the best copy furnished by the organizational source. It is being released in the interest of making available as much information as possible.

- This document may contain data, which exceeds the sheet parameters. It was furnished in this condition by the organizational source and is the best copy available.

- This document may contain tone-on-tone or color graphs, charts and/or pictures, which have been reproduced in black and white.

- This document is paginated as submitted by the original source.

- Portions of this document are not fully legible due to the historical nature of some of the material. However, it is the best reproduction available from the original submission.

LABORATORY SIMULATION OF IMPACT CRATERING WITH HIGH EXPLOSIVES

by Verne R. Oberbeck

Ames Research Center
Moffett Field, Calif. 94035
December 1970

13

Laboratory Simulation of Impact Cratering with High Explosives

Verne R. Oberbeck

Ames Research Center, NASA

Moffett Field, Calif. 94035

ABSTRACT

Impact and explosion craters have been formed at the same scale in the laboratory. Impact craters were produced with cylinders of aluminum of mass 0.4350 gm that were impacted with velocity of 2.0 km/sec and kinetic energy of 8.7×10^9 ergs against quartz sand targets. Explosion craters were produced by detonating 0.150 gm charges of PETN high explosive yielding a chemical energy of 8.7×10^9 ergs at various depths beneath the target surface. Crater size and shape, ejecta plume growth and subsurface deformation have been determined. Measurements of cratering effects show that impact crater formation can be simulated by detonation of the explosive placed at a depth of burst of 6.3 mm ±2 mm ($\lambda = 0.26 \pm 0.10$ for cube root scaling).

Caution should be used in applying these results to estimate kinetic energy of formation of large impact craters because knowledge of projectile velocity might be needed in addition to crater size in order to estimate kinetic energy of formation of the crater using an explosion crater analog.

INTRODUCTION

The role of impact cratering in the production of lunar and planetary surface features has become apparent in recent years. Results of manned and unmanned

lunar missions show that the surface of the Moon is covered at each scale of examination by craters, many of which are impact craters. The earth has also been subjected to bombardment by extraterrestrial bodies which have produced large craters. The roots of these features are preserved in terrestrial rock formations, especially in the older stable shield areas of the Earth. Mariner spacecraft photographs of Mars show that it, too, has been extensively cratered. Thus, knowledge of the mechanics of formation and details of structures of impact craters are of great importance in Astrogeologic studies. However, there are few fresh terrestrial impact craters on the Earth's surface. Therefore, large chemical and nuclear explosion craters have been studied in the past as an aid in interpreting the mechanics of formation of impact craters and for purposes of estimating the kinetic energy of the body that produces a given crater. Studies of this type usually imply that very shallow scaled depth-of-burst explosion craters are similar to craters formed by the impact process [Baldwin, 1963; Shoemaker, 1960].

While studies of large explosion craters have been of value for interpreting gross features of impact craters, the results are limited in their reliability. The lack of fresh impact structures impairs attempts to define features characteristic of large impact craters and the conditions of formation of these craters are unknown. Deep structures beneath both impact and explosion craters can rarely be seen, and most natural impact craters have been formed in target materials which are different from one another and from the material at the sites of the explosion craters that are used as analogs.

The objective of this study is to produce impact and explosive craters in the same target material under controlled laboratory conditions to determine the depth of burst that simulates impact. This approach has the advantage that large numbers of craters can be produced in identical targets for checks on reproducibility of results, and that detailed measurements of cratering effects can be made even in areas beneath the craters. The experimental results show that many of the effects of impact cratering at a given impact kinetic energy can be simulated by burial of an explosive at a specific depth of burst where the explosive energy yield is equal to the impact kinetic energy and the shock wave detonation pressure is equal to the peak impact shock wave pressure.

SIMULATION OF THE IMPACT CRATERING PROCESS
WITH HIGH EXPLOSIVES

Baldwin [1963] provides a good review of the theory of simulation of impact crater formation with high explosives. The main line of reasoning supporting the simulation is that at very high impact velocities the impacting body has kinetic energy/unit projectile mass equal to or greater than the energy content/unit mass of TNT. In addition, pressures and temperatures generated by impact are as high or higher than those occurring when explosives are detonated. Baldwin concludes that simulation of the impact process with high explosives is valid when the dominant mode of energy transfer from projectile to target occurs by shock formation. An example given of an impact that can be simulated by explosives is impact against the earth of a large body with impact velocity at about 9.6 km/sec. As in most studies dealing with simulation of impact

cratering with high explosives, control of chemical or nuclear energy and depth of burst is considered sufficient to simulate an impact event of the same energy level.

However, impact cratering studies in rock [Gault, 1963] and in sand [Braslau, 1970] show that the projectile kinetic energy is partitioned to work to form the crater, to waste heat, to crushing of target material and to kinetic energy of the ejecta. Partitioning is controlled by impact velocity. Thus, in this study, impact velocity is controlled and it is used to calculate the amplitude of the shock wave produced in the target. The density of the explosive is selected to produce a detonation wave pressure equal to the pressure of the shock wave generated by impact. This insures that partitioning of energy is as nearly equal as possible for both events. It is recognized that some of the chemical energy of the explosive is partitioned to an expanding gas ball which is never present during impact cratering and there are other minor differences. However, if chemical and nuclear explosion craters are to be used, as in the past, to simulate impact craters, control of impact velocity in addition to energy and depth of burst of the explosive will insure that detonation pressure can be made equal to peak impact pressure. Thus, energy partitioning is as similar as possible for both events.

The velocity of the impact cratering event simulated in this study at a small scale was 2 km/sec. There is no doubt that energy transfer is accomplished at this velocity and scale by formation of a shock wave in the target because calculations based on the equations of state of aluminum and quartz sand show that pressure developed behind the shock wave in sand is 83 kb. The energy content

of the projectile was 1.97×10^{10} ergs/gm, which is more than one half the energy content/unit mass (3.87×10^{10} ergs/gm) of TNT. The shock wave pressure caused by detonation of the explosive used to simulate impact was 83 kb. Thus, the conditions of this experiment satisfy Baldwin's criteria that energy transfer should occur by formation of a shock wave. An additional requirement, that energy partitioning should be as similar as possible for impact cratering and explosion cratering is insured by setting the shock wave pressure equal for both events.

The energy content/unit mass of the projectile is only comparable to the energy content/unit mass of TNT. Impact of a projectile with higher energy content per unit mass and with velocity as high as 9.6 km/sec was not simulated because impact pressure of the shock wave produced in the sand under this condition would have been greater than 500 kb. The detonation pressure of PETN even at a high packing density of 1.6 gm/cc is only of the order of 230 kb [Cook, 1958]. Thus, it would have been impossible to simulate, even approximately, the pressures developed in the sand. This represents a typical difficulty encountered when attempts are made to reproduce both the energy content/unit projectile mass and target shock wave pressure using high explosives. It was considered important to attempt to simulate the shock wave pressures in the target more accurately than the energy/unit mass of the projectile because of the great effect of impact velocity and target shock wave pressure on impact crater size.

Mechanics of Impact Cratering in Natural Materials

Baldwin [1963] assumes in discussing the simulation of impact cratering that projectile kinetic energy is the important projectile property required to predict crater size. In recent years much of the experimental impact data has been interpreted in this manner. The fluid impact model of Charters and Summers [1959] relates crater size to projectile kinetic energy. For this model, the projectile and target are considered to be the same material and the hydraulic analogy of shaped charge penetration is employed to show that the speed of the material in the fluid shell produced in the target by hypervelocity impact is one half the velocity of the projectile. The radial speed of the fluid shell, expressed in terms of impact velocity, is used with the assumption of equivalence of projectile momentum and the product of mass and speed of the fluid shell to calculate the mass of the fluid shell. This yields the result that the kinetic energy of the fluid shell is one half the kinetic energy of the projectile. The expanding fluid shell is resisted by a deformation stress in the target which is assumed, for simplicity, to be constant during the cratering event. Thus, the kinetic energy of the fluid shell is used to do work against the deformation stress. An important conclusion of the analysis is that the mass displaced from the crater should be directly proportional to the projectile kinetic energy. A review of results of impact cratering in basalt rock and water shows that experimental results have been interpreted through extensions of the theory.

New impact cratering data have shown that some assumptions of the theory are not valid. The projectile momentum is a variable fraction of the target

momentum over most of the experimental velocity range because momentum is also transferred to the crater ejecta. In addition, the radial speed of the fluid shell cannot be used to calculate the mass of the fluid shell from the product of the projectile mass and projectile velocity because only velocity is a vector quantity.

It will be shown that the theory remains useful for describing cratering under conditions of constant impact velocity. In this case, the projectile momentum is a constant fraction of target momentum and the average component of velocity parallel to the axis of impact is a constant fraction of impact velocity. The predictions of the original Charters and Summers theory are valid under these conditions.

Results of impact cratering experiments performed in this study for impact of aluminum spheres against quartz sand are presented and shown to be consistent with the predictions of this restriction of the Charters and Summers theory. Thus, studies of cratering in water, rocks and sand show that impact kinetic energy is of primary importance in determining the size of an impact crater. This provides justification for using explosive charges that yield a given chemical energy to simulate an impact crater formed by a projectile having projectile kinetic energy equal to charge chemical energy.

Impact Cratering in Rocks and Water

Moore et al. [1965] showed that the observed relationship between the mass displaced and the projectile kinetic energy for craters produced in basalt could

be explained by the Charters and Summers theory if it was assumed that the deformation stress in the target is a function of the defect length in basalt. Gault and Moore [1965] generalized and extended this finding to include the dependence of deformation stress on impact velocity. This resulted in a general equation which expresses mass ejected from the target in terms of projectile kinetic energy, E_p:

$$Me \alpha \left(\frac{E_p}{V^m V} \right)^{\frac{3}{3-n}}$$ (1)

where n is the exponent in the relationship between defect length, X, and deformation strength, S: $S = KX^n$; m is a constant and V is impact velocity. Results of cratering in most natural rocks should usually be described by this relationship.

Gault and Moore [1965] reported that for large cratering events in water, where the deformation stress is hydrostatic pressure, an extension of the Charters and Summers theory successfully predicts the experimental results that mass ejected from transient water craters is proportional to $E_p^{3/4}$:

$$Me \alpha E_p^{3/4}$$ (2)

Impact Cratering in Quartz Sand

One hundred forty four impact craters have been produced in this study. Spheres of 2024 aluminum of variable mass and velocity were fired in trajectories normal to the surface of quartz sand targets. The techniques of launching projectiles at velocities greater than 1 km/sec require that special projectile

covers be fabricated for each projectile size, to protect the gun barrel. In practice, this has limited the number of projectiles of different mass that were used in this experiment to five. Although impact velocity could be varied continuously, projectile mass was not. This experimental limitation must be considered in preliminary examination of plots of the data expressing mass displaced in terms of projectile kinetic energy.

Figure 1a shows direct plots of mass displaced as a function of kinetic energy for each of the projectiles with the indicated masses. The position of each line showing the relationship for constant projectile mass is fixed by the particular projectile mass. The results indicate that for any given projectile kinetic energy a continuous series of crater sizes is produced. No relationships, such as those predicted by the Charters and Summers theory, are apparent when the data are plotted as in Figure 1a.

A review of the assumptions involved in the Charters and Summers theory will show that no predictable relationship should result when data are plotted as in Figure 1a; the review will suggest an alternative method of expressing the data which satisfies the assumptions of the theory. When this is done, the experimental results are shown to be consistent with predictions of the theory.

The Charters and Summers theory relates the energy of formation of a single crater to the deformation stress in the target material according to the following equation:

$$K.E._{F.S.} = 2\pi \int_0^r Sr^2 dr \tag{3}$$

where $K.E._{F.S.}$ is the kinetic energy of the fluid shell produced in the target

material by impact, S is the deformation stress and r is final crater radius.

The first assumption is that the projectile and the targets are made of the same

material. Their second assumption comes from the hydraulic analog of shaped

charge penetration for which the speed of the target material is one half the

velocity of the projectile. The third assumption is that the product of the mass

and speed of the hemispherical fluid shell, measured along radials is equal to

the product of the mass and velocity of the projectile. As a result of these

assumptions the kinetic energy of the fluid shell or energy of formation is equal

to one half the kinetic energy of the projectile, E_p. The last assumption is that

the deformation stress is constant during the Formation of the crater. When

these assumptions are made, equation 3 yields, if S is target strength:

$$E_p = kM_d \tag{4}$$

where E_p is the kinetic energy of the projectile and M_d is the mass displaced

from the crater. Gault and Moore [1965] have shown that, if hydrostatic pressure

is the deformation stress, equation 3 simplifies to:

$$E_p = kM_d^{3/4} \tag{5}$$

The assumptions that yield equations 4 and 5 are not valid when data from

craters formed by projectiles of different impact velocity are plotted together.

For these events, projectile momentum is not a constant fraction of target

momentum [Denardo, 1962]. Consideration of the equations of state of aluminum

and quartz sand show that the particle velocity in the target is a nonlinear function

of impact velocity. Thus, both the mass and velocity of the fluid shell are functions of impact velocity. Therefore, the kinetic energy of the fluid shells of craters produced by projectiles of the same mass but different velocities is a function of projectile kinetic energy. For these events, the relationship between size and projectile kinetic energy should not be described by equations 4 or 5. There is another difficulty in relating the data as plotted in Figure 1a to the theory. The theory assumes that a mean value can be used for the deformation stress during a single cratering event and during different cratering events. The shock wave pressure is a function of impact velocity and it is variable for data plotted on any of the lines of Figure 1a. Grine and Fowles [1959] indicate that the dynamic strength of rocks at high pressures is greater than static strength and Moore et al. [1963] have correlated impact data on the basis of change in target strength with confining pressure. Thus, for any of the events represented by data on a given line of Figure 1a, the deformation stress cannot be assumed constant if deformation stress is target strength. The Charters and Summers theory cannot be used to interpret the size energy relationship between impact craters formed by projectiles with different impact velocities.

However, if data for craters produced by projectiles of different mass and the same impact velocity are correlated, the resulting experimental relationship between mass displaced and projectile kinetic energy should be compatible with predictions of the original Charters and Summers theory. Neglecting possible scale effects, craters produced by projectiles having the same impact velocities but different masses transfer a constant fraction of projectile momentum to the

target. The particle velocity in the target is also related to impact velocity by a constant. It can be shown from these properties of impact at constant velocity that the mass of the fluid shell is a constant multiple of projectile mass. Thus, both the mass of the fluid shell and its velocity are related to the projectile mass and impact velocity, respectively, by constants and the formation energy is a constant fraction of projectile kinetic energy for all events. The projectile kinetic energy can be considered a constant multiple of the kinetic energy of the fluid shell in the Charters and Summers theory. For all events, the impact shock wave pressure is the same so a mean value can be assumed for the dynamic strength and density of the material behind the shock wave. This satisfies the second assumption of the Charters and Summers theory that deformation stress is constant. Thus, equation 4 or 5 should apply to craters formed at the same impact velocity.

The data of Figure 1a have been fitted to five equations of the form $M_d = c(E_p)^m$ by the method of least squares. There is one pair of values of c and m for each projectile mass. For each value of projectile mass and impact velocity between 0.5 km/sec and 5 km/sec, in the intervals listed in Figure 1b, projectile kinetic energy was computed. For each velocity value these five values of projectile kinetic energy were used to calculate the corresponding values of mass displaced using the equations fitted from the data of Figure 1a. Thus, for every velocity listed in Figure 1b five pairs of values of mass displaced and projectile kinetic energy are computed. The values of m listed in Figure 1b were then computed from these values, and the data were plotted in Figure 1b.

The data of Figure 1b represent the experimental relationship between mass dis-
placed and projectile kinetic energy for impact craters produced at constant
velocity in the range of impact velocity from 0.5 km/sec to 5 km/sec. The
values of m can now be reasonably expected to agree with predictions of the
original Charters and Summers theory. The data of Figure 1b indicate that for
impact craters produced by projectiles of different masses and constant velocity,
the mass displaced is proportional to the projectile kinetic energy raised to a
power between 0.795 for impact at 0.5 km/sec and 0.877 for impact at 5 km/sec.
Equation 4 predicts that mass displaced from a crater should be proportional to
projectile kinetic energy when deformation stress is target strength and impact
velocity is constant. Equation 5 shows that mass ejected from the crater should
be proportional to the 3/4 power of projectile kinetic energy when deformation
stress is hydrostatic pressure or overburden pressure and impact velocity is
constant.

The relationships shown in Figure 1b where mass displaced is proportional
to projectile kinetic energy raised to a power between 0.795 and 0.877, depending
on the velocity, appear to reflect a transition. The relationships are transitional
between that for cratering in high strength materials where mass displaced is
proportional to projectile kinetic energy and for cratering in materials like water
with negligible strength, where mass displaced is proportional to projectile
kinetic energy raised to the 3/4 power. This behavior must be due to the fact
that both overburden pressure and target strength are important components of
the deformation stress in this range of impact velocity. This is a reasonable

result. When craters are formed in sand, in reduced gravity fields, craters are larger per unit kinetic energy than they are when produced in 1g gravity fields. Explosion craters are also larger per unit chemical energy in reduced gravity fields [Johnson et al., 1970]. Thus, gravity is obviously an important control for cratering in sand. Yet cratering in sand also exhibits effects of target strength because the crater remains intact after formation and never collapses as it does for cratering in water where strength is negligible. However, craters formed in very high strength targets show no dependence of crater size on gravity field. Thus, we should expect, in agreement with results, to obtain a relationship between mass displaced and projectile kinetic energy for cratering in sand that is transitional between that for cratering in water, where strength is of no importance, and cratering in rock where strength is of great importance. The data of Figure 1b suggest that at low velocities target strength is of less importance than at high velocities because mass ejected is more nearly pro-portional to energy raised to the 0.75 power at 0.5 km/sec than at 5 km/sec. As velocity increases, the power of energy in this relationship increases and cratering efficiency decreases. It is thought that this indicates a transition between gravity scaling at low velocities and strength scaling at high velocities. This interpre-tation is supported by the fact that the dynamic strength of materials increases with confining pressure [Grine and Fowles, 1959] and pressure increases with impact velocity. Thus, the shear strength of sand may be so low at low velocity that the energy of formation is used predominantly to do work against gravity. The shear strength may be so high under the conditions of high confining pressure

at high impact velocities that the energy of formation may be used predominantly
to do the work of breaking the bonds between the sand grains induced by high
confining pressures. Other supporting evidence is that data for craters produced
in sand at high velocities (5 km/sec) is closer to data plotted for impact in rock
than is the low velocity data and the power of energy for the high velocity data in the
relationship between mass ejected and energy is nearer to one than for the low
velocity data. However, other effects may contribute to the reduction in the
efficiency of cratering with increasing impact velocity. For example, the per-
centage of projectile kinetic energy wasted as heat in the target may increase
with impact velocity.

A review of impact cratering in rock, water, and sand shows that experi-
mental data can be explained by a model of impact that relates projectile kinetic
energy to target deformation stress for craters produced at the same impact
velocity. Thus, there is experimental and theoretical justification for attempting
to simulate impact crater size as well as other cratering effects by detonating
explosives at various depths of burst if the charges yield chemical energy and
detonation pressure equal to the kinetic energy and shock wave pressure of
impact.

Relationship Between Energy and Size for Explosion Craters

For explosion craters, it is well known that linear crater dimensions,
ℓ scale according to the relationship: $\ell = aW^n$ where a is a constant, W is
taken as either the weight or the energy of the charge, and the value of n is
uncertain and may vary between values of 1/2.5 and 1/4 dependent on target

properties [Sun, 1970]. But, efficiency of cratering also depends on the depth of burst of the charge. As the charge is buried at progressively greater depths, cratering efficiency increases until an optimum depth of burst is reached. Charges buried at greater depths produce smaller craters. Thus, Baldwin [1963] has derived equations relating crater diameter to energy for various values of scaled depth of burst craters ($\lambda = h/W^{1/3}$ where h is depth of burial of the charge and n is taken as 1/3). Evidence is also presented that shallow scale depth of burst explosion craters ($\lambda = 0.1$) simulate impact craters. The equation for this scaled depth of burst is then used to compute the energy and mass and velocity required to form an impact crater of a given size. Because Sun [1970] reported finding 41 published values of n for the scaling equation $1 = aW^n$ used to describe experimental explosion craters and because it is uncertain which value of n is a basic reflection of the cratering process, I report results here only in terms of depth of burst of the charge rather than scaled depth of burst except for those specific comparisons with earlier results, which have been reported in terms of scaled depth of burst. However, mean depth of burst data can be easily used to compute scaled depth of burst after a value for the exponent is selected by the reader if the weights of the charges of PETN explosive are converted to equivalent weights of TNT in pounds.

Summary

Consideration of the role of kinetic energy and chemical energy in the formation of impact craters and explosion craters implies that an impact event which has kinetic energy E, and impact velocity which produces a target shock

wave of amplitude P can be simulated by burial and detonation of a charge of explosive that yields detonation pressure P and chemical energy equivalent to the kinetic energy of impact. One characteristic of high explosives limits the selection of the impact velocity that is to be simulated: if a high enough impact velocity is selected to be simulated, the pressures developed behind the shock wave in the target can be far above those developed by explosives, even at their highest packing density. For this reason, a moderate impact velocity of 2 km/sec has been simulated, because the peak impact pressure developed in the sand by the impact of an aluminum cylinder at this velocity is 83 kb. This pressure is equivalent to the detonation pressure of PETN high explosive when it has a packing density of 1 gm/cc, the packing density of charges used in this study.

EXPERIMENTAL CONDITIONS

Impact craters and explosive craters were formed in quartz sand with grain size distribution shown in Figure 2. Craters were formed inside a chamber 2.4 meters in diameter and 3 meters in height that was evacuated to air pressure of 1 mm ±0.5 mm. The chamber was large enough to prevent any of the material excavated from the target to be reflected from the chamber walls back into the crater. All targets were 100% quartz sand except for those used for study of subsurface deformation. These contained 0.16% by weight of powered epoxy resin.

Seven impact craters were formed in this simulation study. They were produced by cylinders of aluminum with mass = 0.4350 gm ±0.020 gm which impacted

the quartz sand at impact velocity of 2.00 km/sec ±0.04 km/sec. Calculations using the equations of state of quartz sand, 2024 aluminum, and the impedance match solution given in the Compendium of Shock Wave Data edited by M. Van Theil [1966] show that impact of 2024 aluminum in quartz sand at 2 km/sec produces a shock wave in the sand with pressure amplitude equal to 83 kb. The ratio of projectile diameter to projectile length was 0.80 and the projectile kinetic energy was 8.7×10^9 ergs $\pm 0.7 \times 10^9$ ergs. Six craters were produced in 60 cm diameter cast aluminum target containers that were 15 cm deep. The crater formed for the study of subsurface deformation was produced in a 60 cm square wooden box, 15 cm deep.

Cylindrical aluminum projectiles were launched in protective discs of plastic by a conventional powder gun similar to a high powered rifle. This gun, mounted on a rail, can be rotated about the impact chamber. The protective plastic disc was slit at right angles in planes parallel to the longitudinal axis of the projectile so that spin imparted by the gun barrel rifling separated the plastic pieces from the projectile after launch and laterally deflected them to a catching plate. After launch, the projectile entered the velocity chamber. A photodiode triggered a high voltage spark which served as a light source to produce a shadowgraph of the projectile in flight. The high voltage discharge triggered a time interval meter which recorded time elapsed since launch. Projectile positions were measured referenced to a fiducial bar and differences in elapsed time after launch yielded estimates of impact velocities with accuracy of ±1%. All impact craters were formed with impact kinetic energy between 8.1×10^9 ergs and 9.5×10^9 ergs.

Seven explosive craters were formed at each of 4 different shallow depths of burst using the high explosive pentaerythritol tetranitrate (PETN). The center of the charge for each of the depths of burst less than 10 mm were: 0 mm ±1 mm, 3.2 mm ±1 mm, 6.3 mm ±1 mm, and 9.5 mm ±1 mm. Four explosion craters each were formed at the depths of burst: 14.3 mm ±1 mm, 27.0 mm ±1 mm, 39.7 mm ±1 mm, 52.5 mm ±1 mm, 65.2 mm ±1 mm, and 77.8 mm ±1 mm. All craters were produced in target containers similar to those described for the impact craters. Each of the cylindrical charges was 6.4 mm in diameter and 4.6 mm long and detonation was initiated by high voltage explosion of a bridge-wire embedded in the explosive. Packing density of the explosive was 1 gm/cc. For the explosive PETN, this yields a detonation wave pressure of 83 kb [Cook, 1958]. The weight of the charge was 0.150 gm for all craters. According to data given by the Kirk and Othmer Encyclopedia of Chemical Technology [1965] the heat of detonation of PETN at a packing density of 1.7 gm/cc is 1385 cal/gm. The results of Cook [1958] show that this value is accurate within ±1.5% for the same material packed at 1.0 gm/cc. Therefore, for this study a value of 1385 cal/gm is assumed for the explosive. Thus, all charges of 0.150 gms used here provide chemical energy available for cratering equal to 8.7×10^9 ergs. This energy is equal to the kinetic energy of the aluminum projectiles which produced the impact craters. The detonation pressure is also equal to the pressure behind the shock wave produced in the sand at the time of impact. In order to insure that explosion of the bridge wire did not contribute significantly to cratering, the wire was exploded in sand several times. Cratering was not observed. A series of trial cratering experiments was also

performed to demonstrate that the target containers used were large enough to prevent edge effects that might interfere with crater growth. These experiments included measurement of crater dimensions in target containers much larger than those routinely used and observation of control markers beneath craters formed in the standard target containers. No interference effects were observed.

MEASUREMENTS OF CRATERING EFFECTS

For impact craters formed in sand targets at constant velocity, crater volume depends on the kinetic energy of the impacting body raised to some power between 0.75 and 1.0. Most interpretative studies of large impact craters have also assumed that kinetic energy is important in determination of crater dimensions. For explosion craters, size depends on the total yield of chemical energy of the explosive and depth of burst of the charge. Thus, apparent crater diameter is an obvious cratering effect to be measured in simulation of impact crater formation by detonating explosives buried at different depths. For craters formed in sand, crater shape depends on the impact velocity. Because the velocity has been controlled in this experiment, crater shape is an important cratering effect to be observed. Both size and shape of impact and explosion craters have been determined by obtaining two profiles passing through each crater center and intersecting at an angle of 90°. For each profile of each explosion and impact crater, a rectangular coordinate system was superimposed on the profile so that the coordinate (0,0) was at the crater bottom. For each interval of +X and -X of 1 cm, the Y coordinate of intersection with the crater wall was determined. For all impact craters and for all explosion craters formed at the same depth of burst, the mean and two

standard deviations of each of these coordinates were determined and an average profile was constructed. These profiles are the data for determination of which depth of burst simulates impact on the basis of crater size and shape.

The details of the growth of both impact and explosion crater ejecta plumes have been determined in this study from study of high speed motion pictures of cratering events. The nature of the ejecta growth for explosion craters is related to chemical energy, target shock wave geometry and depth of detonation. For those events where the charge is deeply buried, the ejecta grows as an expanding bubble which finally is vented before material falls back into the crater. This ejecta growth pattern reflects the presence of both the spherical shock wave and the expanding gas ball, which is characteristic of craters produced by deeply buried charges. Those explosion craters formed by charges placed at the surface are characterized by growing ejecta fans that are vented at once and never possess bubble-like ejecta plumes. They are similar to the ejecta plume patterns of impact which are the surface reflections of hemispherical-shaped shock waves developed in the target by the impacting body. Because ejecta plume growth is a surface manifestation of the charge energy, the shock wave geometry developed in the target, and depth of detonation it is considered a definitive cratering effect to be measured for the simulation study.

High speed motion pictures of ejecta plumes of impact and explosion craters were obtained using a 16 mm high speed framing camera with typical framing rates of 8000 to 10,000 frames/sec. After a photographic record was obtained, a calibration curve relating elapsed time to photograph frame number was derived

from millisecond marks recorded on the film. Those frames corresponding to times elapsed from impact or explosion of 2, 10, 20, 40, 60, 80, 100, 120, and 140 msec were projected for tracing of the ejecta plumes at these elapsed times. These times are accurate within ± 100 μsec. The point on the target surface that corresponded to impact for each impact crater and ground zero for each explosion served as the (0, 0) coordinate of a rectangular coordinate system that was super-imposed on each of these ejecta plume diagrams. Then, for fixed vertical inter-vals, the +X and -X coordinates of intersection with the lateral boundaries of the ejecta plumes were determined for each of the ejecta plume positions at each time interval. The mean and two standard deviations of each of these coordinates were determined for the impact craters and for explosion craters formed at the same depth of burst. The resultant average ejecta growth patterns can be used for determining which depth of burst explosion crater simulates impact.

The magnitude and direction of subsurface deformation that occurs beneath impact craters is a function of both the kinetic energy and velocity of the body that impacts. This can be realized at once if it is considered that craters formed at higher energy are bigger than those formed at lower energy and low velocity projectiles burrow into a target but high velocity projectiles are fragmented and ejected from the crater. The magnitude and direction of subsurface deformation for explosion craters is a function of chemical energy, depth of burst and probably detonation pressure. For example, explosion craters formed by charges buried very deeply, contain large quantities of mixed fallback material beneath the surface of the crater bottom. The subsurface structure is much different than

that of craters formed at shallow depths of burst which contain little if any fall-back material. The degree and direction of subsurface particle flow beneath impact and explosion craters reflect the basic mechanisms of the particular condition of cratering considered and therefore are important cratering effects to be measured in a simulation study.

Diehl and Jones [1964] described a tracer technique for observing particulate flow beneath large terrestrial explosion craters. The method involves placement of marker cans in colored sand columns in arrays surrounding ground zero. After crater formation, marker cans remaining in the target are located and surveyed when the crater is sectioned. The study showed that a vector diagram could be constructed to connect initial particle position with final particle position for each of the marker positions beneath the crater. This diagram was shown to be similar to a scaled down plot of the theoretical hydrodynamic velocity vectors calculated by Brode and Bjork [1960] for a megaton surface burst. The method also was useful for showing shear zones and the amount of compaction beneath explosion craters. Their results indicate that the tracer technique is a valuable tool for showing details of the cratering mechanism. This technique has been modified for use in small scale laboratory experiments. Multicolored sand columns are positioned in the loose sand targets along a transverse 5 cm thick segment of the target at regular intervals. Each column consists of alternating 6.3 mm thick red and blue colored sand zones. The sand contains 0.16% by weight of powdered epoxy resin. After the crater is produced, the entire target is placed in an oven and baked at 150°C. The indurated target is then cut and detailed flow beneath

the crater can be observed. Figure 3 shows a section of a target that has been cut directly after fabrication and baking. This illustrates the initial position of all discrete colored sections of sand. The horizontal control in positioning each discrete element of colored sand is about the median dimension of the individual sand grains (400μ). Targets such as this provide a valuable tool for determining which depth of burst explosion crater simulate the impact crater, because sub-surface deformation is intimately related to cratering energy, shock wave pressure and geometry and shock wave decay.

For the impact crater and for each explosion crater, the final positions of each discrete zone of colored sand in a plane passing through crater center have been traced from photographs of the sectioned targets. Comparison of these diagrams will determine which depth of burst explosion crater produces sub-surface deformation similar to that produced by impact.

EXPERIMENTAL RESULTS

Explosion Crater Profiles and Impact Crater Profiles

Figure 4 shows a series of average profiles in black, each of which repre-sents craters produced by charges detonated at the same depth. Each of the first four profiles of Figure 4 represents the average profile of six craters formed at one of four different specified depths of burst less than or equal to 9.5 mm ±1 mm. The average profiles for those craters formed at depths of burst greater than 9.5 mm ±1 mm represent the average profiles of only four craters produced at each depth of burst. The profiles of all explosion craters of Figure 4 are superimposed

on the average grey profile of six craters formed by impact of cylinders of 2024 aluminum.

Study of profiles of the explosion craters shows that as charges are buried at greater depths, the crater becomes larger. At greater depths of burst, coupling between the explosive and target material is better than for shallow depths of burst where gas products of the explosion are vented. Crater shape also changes with increasing depth of burst. The crater formed by the surface burst has a nearly spherical segment shape. Those formed at mean depths of burst of 3.2 mm ±1 mm and 6.3 mm ±1 mm and 9.5 mm ±1 mm have crater shapes transitional between the spherical segment shape and the conical shape. Those craters produced by charges buried at depths of burst greater than 9.5 mm ±1 mm are nearly conical in shape. The spherical segment shape of the craters formed at mean depth of burst of 0 mm ±1 mm is thought to reflect best the geometry of a crater formed predominantly by relaxation of a hemispherical shock wave produced by detonation. At this shallow depth of burst, cratering due to both gas acceleration and target compression is less than for any of the other explosion craters. The main cratering mechanism is the formation of rarefaction waves at the target-free surface which relaxes the high pressures in the target by accelerating the target material into ballistic trajectories. For craters formed at depths of burst greater than about 9.5 mm ±1 mm, crater shape is conical as a result of slumping of crater walls. Cratering efficiency has increased enough at these depths that gas acceleration and compaction of target materials form a spherical cavity beneath the target surface during crater

formation. The energy available for cratering is sufficient to remove most of the materials set in motion, but some material slides back toward the crater center forming straight internal crater walls. In addition, as more and more material is set in motion at increasing depths of burst by the expanding gas ball and rarefaction waves, more material falls back into the target. Thus, these craters are shallower and at extreme depths of burst, a central peak is sometimes formed from chaotically mixed fallback material.

The average profile of the six impact craters also reflect the mechanics of formation. Differences between impact and explosive crater formation are that there is no formation of a gas ball for impact cratering and a hemispherical shock wave is formed rather than the spherical shock wave that is formed in craters produced by deeply buried explosive charges. Thus, the profile of the impact crater matches the profile of the shallow depth of burst explosion crater with mean depth of burst of 6.3 mm ±1 mm. For this event, the gas ball vents early in cratering and the shock wave geometry must approximate the impact produced shock waves because its source is near the target surface. The 0 mm mean depth of burst explosion crater fails to simulate the formation of the impact crater mainly because the crater is too small because of poor coupling between the explosive charge and the target. Figure 5 shows a plot of diameter to depth ratios for craters produced by various depths of burst of the charge and for the impact craters. The diameter to depth ratio of the 0 mm mean depth of burst explosion crater is considerably greater than that for the impact craters. This reflects poor coupling between charge and target; there is less compression

beneath the target for the surface burst crater than is present beneath impact craters. Diameter to depth ratios of explosion craters formed at depths of burst between 3 mm and 14 mm are the same and are most similar to the diameter to depth ratio of the impact craters. Because the ratio is the same for a large range in depth of burst, diameter to depth ratio is an insensitive criterion for simulation. Inspection of the average profiles of impact craters and explosion craters indicates that the charge buried at mean depth of burst of 6.3 mm ±1 mm produces a crater that exactly matches the size and shape of the impact crater.

Ejecta Plume Diagrams for the Impact Craters and the Explosion Craters

Figure 6 shows the mean boundaries of the ejecta plumes at specified elapsed times from impact or detonation for impact craters and explosion craters formed by charges detonated at a given depth of burst. For each event, each set of ejecta positions for the elapsed times shown is the average position of the ejecta plumes. The horizontal flags show two standard deviations of the lateral positions of the ejecta plume for each of the specified times. Diagrams showing the ejecta growth pattern in black for explosion craters formed at all depths of burst are superimposed on the diagram showing the average ejecta plume growth pattern of the impact crater which is repeated in the figure in grey.

Those explosion craters formed by deeply buried charges (≥27.0 mm ±1 mm) all exhibit bubble-like ejecta plumes, especially early in the cratering events. For example, the shape of the ejecta plume 2 msec after detonation for the 39.7 mm ±1 mm mean depth of burst explosion crater is dome-like. For craters produced by charges buried at depths of burst greater than 39.7 mm, the bubble persists for

longer and longer periods of time. Formation of the bubble is due to the combined effect of the spherical shock wave and the accelerating spherical gas ball. Disappearance of the bubble late in the cratering event coincides with venting of gases above the target surface. The bubble persists later in cratering for deeply buried charges than for shallow depths of burst because there is more material set in motion in near vertical trajectories. All explosion craters characterized by bubble-shaped ejecta plumes (those formed at depths of burst greater than or equal to 27 mm) do not simulate the effects of impact cratering because impact crater ejecta plumes never have this appearance. The explosion crater formed by the 0 mm mean depth of burst charge does not possess a bubble-shaped ejecta plume at any time during the event because the products of the explosion vent at once and the shock wave geometry in the target is approximately hemispherical. However, for these craters, the slopes of the lateral boundaries of the ejecta plumes are less than for impact. Those explosion craters formed at intermediate depths of burst also vent very soon after impact, but coupling between target and explosive is better as evidenced by greater crater size.

Study of all of the diagrams of average ejecta positions at the indicated elapsed times from impact and explosion shows that none of the patterns of ejecta growth of the explosion craters formed at the indicated depth of burst exactly duplicates the pattern of ejecta development of the impact crater. The explosion craters that exhibit an ejecta growth pattern most like that of impact on the basis of positions of the ejecta plume lateral boundaries are those formed by the charge detonated at a mean depth of burst of 6.3 mm ±1 mm. The pattern

differs from the ejecta pattern of the impact crater only because the position of the lateral boundaries of the plume are translated further from the point of detonation for the explosion craters. The difference is less for craters produced at this depth of burst than for any other depth. However, the slopes of the ejecta position boundaries of the explosion crater formed by the charge placed at a depth of 9.5 mm ±1 mm are most similar to those of the impact crater. Figure 7a shows a plot of the slopes of the straight portions of the ejecta envelopes as a function of time in milliseconds for the diagrams of the impact crater ejecta plumes and for each of the explosion crater plumes. The slopes of the ejecta boundaries late in crater-ing are most like those of the impact event for the crater produced by the charge buried at 6.3 mm ±1 mm. However, Figure 7b shows that the sum of the squares of the deviations of the slopes of the ejecta plume of the explosion craters from the slopes of the ejecta plumes of the impact crater for all ejecta plume positions is less for the 9.5 mm ±1 mm depth of burst explosion crater than for any of the other explosion craters.

Subsurface Particle Flow for the Impact Crater and the Explosion Craters

Deformation produced beneath the explosion craters and impact craters formed in quartz sand has been studied by using special targets containing colored columns of sand. An uncratered target indurated directly after fabrication is shown in Figure 3. A section through an impact crater is shown in Figure 8a. Deforma-tion beneath the crater is characterized by appreciable compression. This can be confirmed by tracing the discrete elements of sand near the bottom of the target across the target. Examination of the area beneath the crater shows that the direction

of net particle flow grades from radial beneath the impact point to tangential near the crater rim. Beneath the crater, at intermediate positions, the flow is nearly horizontal and it is directed away from the crater center. Subsurface flow for the impact crater is always downward near the crater center. The vertical component of flow becomes positive away from the crater center. There never is a horizontal component of flow that is directed toward the crater center for the impact crater. However, horizontal components of flow directed toward crater center do occur for some explosion craters produced by deeply buried charges. Figure 8b shows a section of a target containing an explosion crater formed by a charge placed at mean depth of burst of 6.3 mm ±1 mm, that depth of burst explosion crater found to simulate the impact crater on the basis of size and shape and ejecta plume growth. The deformation pattern beneath this explosion crater is remarkably similar to the deformation pattern beneath the impact crater of Figure 8a. The same radial compression beneath the crater center is noted and there is a positive horizontal component of particle flow beneath the sidewalls of the crater as well as a positive vertical component of flow near the crater rim. Deformation patterns beneath the explosion craters formed at greater mean depths of burst are much different, containing chaotic mixing structures and slump structures. These features are caused by fallback of the material with low initial velocities that produce the dome-like ejecta plume patterns discussed earlier.

Positions of the discrete elements of colored sand in the sections of targets of all explosion craters and the section of the target containing the impact crater

have been traced from photographs similar to those of Figure 8. These diagrams

are presented in Figure 9. Tracings of half sections of the impact crater are re-

peated in the left half of the figure in a grey tone. One half sections of explosion

craters formed at various depths of burst are shown in black on the right half of

the figure. Inspection of the sections shows a continuous variation of structure

for the explosion craters as the charge is buried deeper and deeper. Deformation

of the discrete elements of colored sand beneath the 0 mm and 3.2 mm depth of

burst explosion craters is similar in direction to that observed beneath the impact

crater but magnitude of particle flow is less for these craters than for the impact

crater. The magnitude and direction of particle flow beneath the 6.3 mm ±1 mm

mean depth of burst explosion crater exactly match that beneath the impact crater.

Deformation of the discrete colored sand elements beneath the explosion craters

formed at mean depths of burst greater than 6.3 mm ±1 mm differs in direction

and magnitude from those observed beneath the impact crater. For example, the

explosion craters formed at mean depth of burst equal to 9.5 mm ±1 mm contain a

nearly horizontal component of flow near the crater bottom and the crater formed

at a mean depth of burst of 14.3 mm ±1 mm is characterized by slight slump

structures which occur as recurvatures of the colored columns toward crater

center near the crater wall. As charges are buried deeper and deeper, the

tendency for slumping increases until the extreme mixing and slump structures

similar to those of the 52.5 mm ±1 mm mean depth of burst explosion craters

develop.

It is concluded on the basis of study of subsurface deformation exhibited by the diagrams of Figure 9 that the 6.3 mm ±1 mm depth of burst explosion craters is characterized by subsurface deformation exactly the same as that observed beneath the impact crater.

Discussion

It has been demonstrated in this study that, on the basis of crater size and shape and subsurface structure, impact craters formed in the laboratory by impacting cylinders of 2024 aluminum of mass 0.4350 gm against a quartz sand target with impact velocity equal to 2.0 km/sec and impact kinetic energy of 8.7×10^9 ergs can be simulated by detonation of a 0.150 gm charge of the high explosive PETN which yields chemical energy equal to the kinetic energy of the impact event, if the mean depth of burst of the charge is equal to 6.3 mm ±2 mm. Ejecta plume growth patterns of explosion craters formed at 6.3 mm ±1 mm and 9.5 mm ±1 mm are most similar to those of impact craters. Since crater size and shape and structure are of primary interest, it is concluded that impact is simulated by the 6.3 mm ±2 mm explosion crater. If it is assumed that dimensions of explosion craters scale according to the cube root of the charge weight of TNT in pounds and if the charge weight of PETN is converted to equivalent weight of TNT, the results of this study show that explosion craters formed at scaled depths of burst = $h/W^{\frac{1}{3}}$ = 0.26 ±0.10 simulate formation of impact craters. In this ratio, h is the mean depth of burial of the explosive charge in feet and W is the weight in pounds of TNT.

Caution must be used in using explosion craters formed at this scaled depth
of burst as analogs for calculating conditions of formations of impact craters.
In addition to the uncertainty of the selection of the exponent of W that should
be used [Sun, 1970], there is a more serious difficulty that may cause error
when explosion craters are used as analogs for estimating the kinetic energy,
and other conditions of formation of a given impact event. Laboratory results
indicate that, without knowledge of either impact velocity or projectile mass,
which can usually not be obtained in nature, kinetic energy cannot be estimated
from crater size alone. Projectiles of different masses but with the same kinetic
energy produce craters of different size in quartz sand (Figure 1a). Impact
craters formed by projectiles with the same kinetic energy but different pro-
jectile mass-projectile velocity combinations display different subsurface flow
as well as a difference in size. Figure 10 shows a photograph of a cross section
of a crater produced by an aluminum projectile with the same kinetic energy of
8.7×10^9 ergs as the impact crater simulated by the explosive charge, but the
projectile mass was 1.60 gm and the impact velocity was 1.04 km/sec. The
mass of the projectile used in the simulation study was 0.4350 gm and the impact
velocity was 2 km/sec. A photograph of the section of the crater produced at
2 km/sec is shown in Figure 8a. The structures beneath these two craters are
very different. For the crater of Figure 10 formed by the larger projectile at
the lower velocity, the projectile burrowed into the target and entrained target
material behind it. This can be confirmed by observation of the colored columns
of sand that curve inward behind the projectile in the target shown in Figure 10.

The projectile of mass 0.4350 gm that produced the crater shown in Figure 8a did not penetrate beneath the crater bottom and the subsurface structure is different. Crater shape is also different and the crater is 20% smaller than the crater produced at lower velocity.

There is evidence that the difference in size and subsurface deformation for craters produced at the same kinetic energy but different projectile mass and velocity combinations is due to the velocity difference instead of the change in projectile mass or size and the resulting changes in the ratio of projectile size to median sand grain size. Three craters have been produced at the same kinetic energy of 8.7×10^9 ergs with projectiles of mass 0.4350 gm and diameter 6.35 mm in three sand targets of different median grain size. For these events, the range in variation of the ratio of projectile diameter to median sand grain size was from 15.9 to 51.5. The maximum variation in crater diameter for these events was 3%. This is considerably less than the 20% difference in crater diameter for the craters of Figures 8a and 10 where the ratio of the projectile diameter to the median grain size only changed from 17 for the crater of Figure 8a to 25.4 for the crater of Figure 10. The results suggest that neither the projectile size nor the ratio of projectile size to sand grain size is the cause of either the change in subsurface deformation or crater diameter for craters produced by projectiles with the same impact kinetic energy but with different masses and velocities. On the other hand, the importance of the role of impact velocity for the production of craters of different size by projectiles with different velocity but equal kinetic energy, can be easily understood. Impact craters produced at higher velocities deposit a

larger fraction of projectile kinetic energy as heat in the target and the dynamic

target strength is higher for impact at high velocity. Thus, less energy available

to do work against higher stress produces a smaller crater. As discussed earlier,

this interpretation is supported by the experimental results plotted in Figure 1b.

The cause of the decrease in impact crater size with increasing velocity for

constant projectile kinetic energy may not be known with certainty, but, because

it occurs, there may be error in using explosion crater analogs to estimate the

conditions of formation of impact craters including the projectile kinetic energy.

Had this effect not occurred the procedure that would be used to determine the

kinetic energy of the projectile that forms any given terrestrial impact crater

would be straightforward. The results of this study have shown, assuming cube

root scaling for explosion craters, that explosion craters formed at scaled depths

of burst of 0.26 ±0.1 simulate impact crater formation at 2 km/sec. Thus, kinetic

energy could be computed from crater diameter from equations such as those

presented by Baldwin [1963] for explosion craters produced at scaled depth of

burst equal to 0.26 ±0.1. However, the data of Figure 1b show that for impact

velocities between 0.5 km/sec and 5 km/sec there are a range of crater diameters

that can be produced at the same projectile kinetic energy. Use of a 0.26 scaled

depth of burst explosion crater analog could therefore yield variable estimates

of projectile kinetic energy for impact craters produced at different velocities

and the same projectile kinetic energy. It is not likely that this would cause large

errors in estimates of projectile kinetic energy for large terrestrial impact craters.

Most of these craters have probably been produced by bodies impacting at velocity

well in excess of 5 km/sec. While the velocity effect is still present at 5 km/sec, the data of Figure 1b show that the difference in crater size due to a difference in impact velocity for a given projectile kinetic energy has become very small at 5 km/sec. It is likely that differences in crater sizes are even less at higher velocity. However, kinetic energy of formation of large terrestrial impact craters can only be approximated from diameter measurement of impact craters and known relationships between crater diameter and chemical energy for explosion craters formed at scaled depths of burst of 0.26 ± 0.1. More exact solutions will require additional experimental knowledge of the exact scaled depth of burst required to simulate a given impact crater formed at a specific velocity and characterized by a specific target shock wave pressure.

REFERENCES

Baldwin, R. B., "The Measure of the Moon," The University of Chicago Press, 1963.

Braslau, D., "Partitioning of Energy in Hypervelocity Impact Against Loose Sand Targets," J. Geophys. Res., 75, pp. 3987-3999, 1970.

Brode, H. L., and Bjork, R. L., "Cratering from a Megaton Surface Burst," Rand Corp., RM 1600, 1960.

Charters, A. D., and Summers, J. L., "Some Comments on the Phenomena of High Speed Impact," Paper presented at the Decennial Symposium, U.S. Naval Ord. Lab., White Oak, Silver Spring, Maryland, May 26, 1959.

Cook, M. A., "The Science of High Explosives," Reinhold Publishing Corp., New York, Chapman & Hall, Ltd., London, 1958.

Compendium of Shock Wave Data, L. R. L., UCRL-50108, Edited by Van Thiel, M., Kasuboo, A. S., Mitchell, A. C., and Davis, V. W., 1966.

Denardo, B. P., "Measurements of Momentum Transfer from Plastic Projectiles to Massive Aluminum Target at Speeds up to 25,000 Feet Per Second," NASA Tech. Note D-1210, 1962.

Diehl, C. H. H., and Jones, G. H. S., "A Tracer Technique for Cratering Studies," J. Geophys, Res., 70, 305-309, 1964.

Gault, D. E., and Heitowit, E. D., "The Partition of Energy for Hypervelocity Impact Craters Formed in Rock," Proceedings of the Sixth Hypervelocity Impact Symposium, Vol. 3, Aug., 1963.

Gault, D. E., and Moore, H. J., "Scaling Relationships for Microscale to Megascale Impact Craters," Proceedings of the 7th Hypervelocity Impact Symposium, Vol. 4, Experiments, February, 1965.

Grine, D. R., and Fowles, G. R., "The Attenuation of Shock Waves in Solid Materials with Seismic Applications," Third Symposium on Rock Mechanics, Colorado School of Mines Quarterly, Vol. 54, 1959, pp. 251-269.

Johnson, S. W., Smith, J. A.; Franklin, E. G., Moraski, L. K., and Teal, D. J., "Gravity and Atmospheric Pressure Effects on Crater Formation in Sand," J. Geophys. Res., 74, pp. 4838-4850, 1970.

"Kirk, Othmer, Encyclopedia of Chemical Technology," 2nd Edition, Vol. 8, Edited by Mark, F., McKelter, J., Jr., Othmer, F., and Stutden, A., Interscience Publishers, a Div. of John Wiley and Sons, Inc., New York, London, Sydney, 1965.

Moore, H. J., Gault, D. E., and Heitowit, E. D., "Change of Effective Target Strength with Increasing Size of Hypervelocity Impact Craters," Proceedings of the 7th Hypervelocity Impact Symposium, Vol. 4, Theory, February, 1965.

Moore, H. J., MacCormack, R. W., and Gault, D. E., "Fluid Impact Craters and Hypervelocity High Velocity Impact Experiments in Metals and Rocks," Proceedings of the Sixth Hypervelocity Impact Symposium, Vol. 3, Aug., 1963.

Shoemaker, E. M., "Penetration Mechanics of High Velocity Meteorites, Illustrated by Meteor Crater Arizona," International Geological Congress, XXI Session, Norden, 1960, part XVIII, Structure of the Earth's Crust and Deformation of Rocks, Copenhagen, 1960.

Sun, J. M. S., "Energy Counter Pressure Scaling Equations of Linear Crater Dimensions," J. Geophys. Res., 75, 2003-2023, 1970.

FIGURE CAPTIONS

Figure 1a - Mass ejected from impact craters formed by aluminum spheres
plotted as a function of projectile kinetic energy for projectiles of
constant mass and variable velocity.

Figure 1b - Mass ejected from impact craters formed by aluminum spheres
plotted as a function of projectile kinetic energy for projectiles of
variable mass and constant impact velocity. These curves have
been derived from the data of Figure 1a.

Figure 2   - Grain size distribution of quartz sand in which explosion craters
and impact craters were formed.

Figure 3   - Photograph of an uncratered colored column target that has been
indurated and sectioned after fabrication.

Figure 4   - Average profile of six impact craters shown in grey and average
profiles of explosion craters formed by detonation of charges at
different depths of burst shown in black. Error bars are two
standard deviations of the measurement of position of height of the
crater surface above the crater bottom. Note that explosion craters
produced by charges placed at 6.3 mm ±1 mm have profiles similar
to the profile of the impact crater.

Figure 5   - Ratio of rim crest crater diameter to rim crest crater depth for
explosion craters formed by charges placed at the indicated depth
of burst and for impact craters.

Figure 6   - Positions of the average lateral boundaries of ejecta plumes for various times during crater growth for impact craters (shown in grey) and for explosion craters formed by charges detonated at the indicated depths of burst.

Figure 7a - Slopes of the straight portions of the ejecta plumes plotted as a function of cratering time in milliseconds for the impact crater and explosion craters formed at the indicated dep'.hs of burst.

Figure 7b - Sum of the squares of the deviations of the slopes of the ejecta plumes of explosion craters from the slopes of the ejecta plumes of the impact crater.

Figure 8a - Section of impact crater formed in a colored column sand target by a cylinder of aluminum of mass 0.4350 gm, impact velocity of 2.0 km/sec, and projectile kinetic energy equal to 8.7×10^9 ergs.

Figure 8b - Section of a colored column target containing an explosion crater formed by detonation of a PETN charge that yields 8.7×10^9 ergs chemical energy placed at mean depth of burst of 6.3 mm ±1 mm below the target surface.

Figure 9   - Diagrams showing the final positions of discrete elements of colored sand beneath an impact crater and explosion craters produced by charges placed at different depths of burst. Flow beneath the impact crater is shown by the repeated diagram on the left which is for one half of the impact crater. One half sections of the explosion craters formed at different depths of burst are shown on the right half of the diagram. The explosion crater produced by the charge placed at burst depth of 6.3 mm ±1 mm provides the best simulation of flow observed beneath the impact crater.

Figure 10 - Photograph of a cross section of an impact crater produced by impact of aluminum cylinder with mass = 1.60 gm, impact velocity = 1.04 km/sec, and impact kinetic energy = 8.7×10^9 ergs.
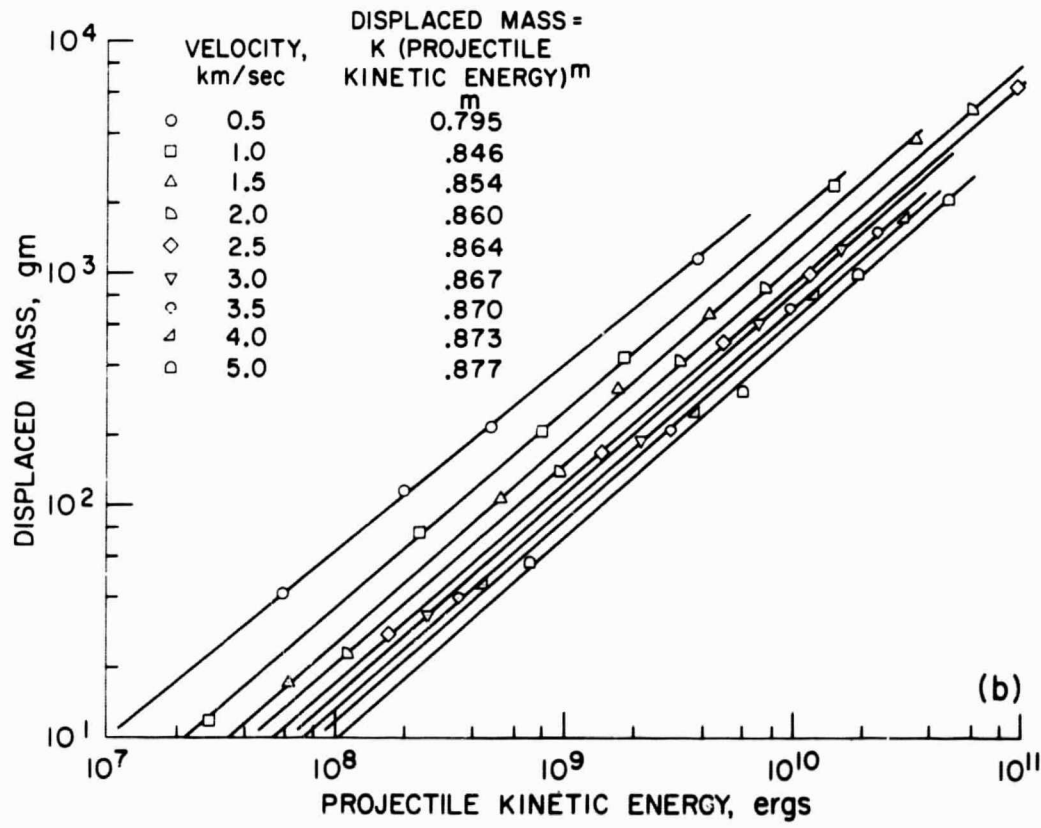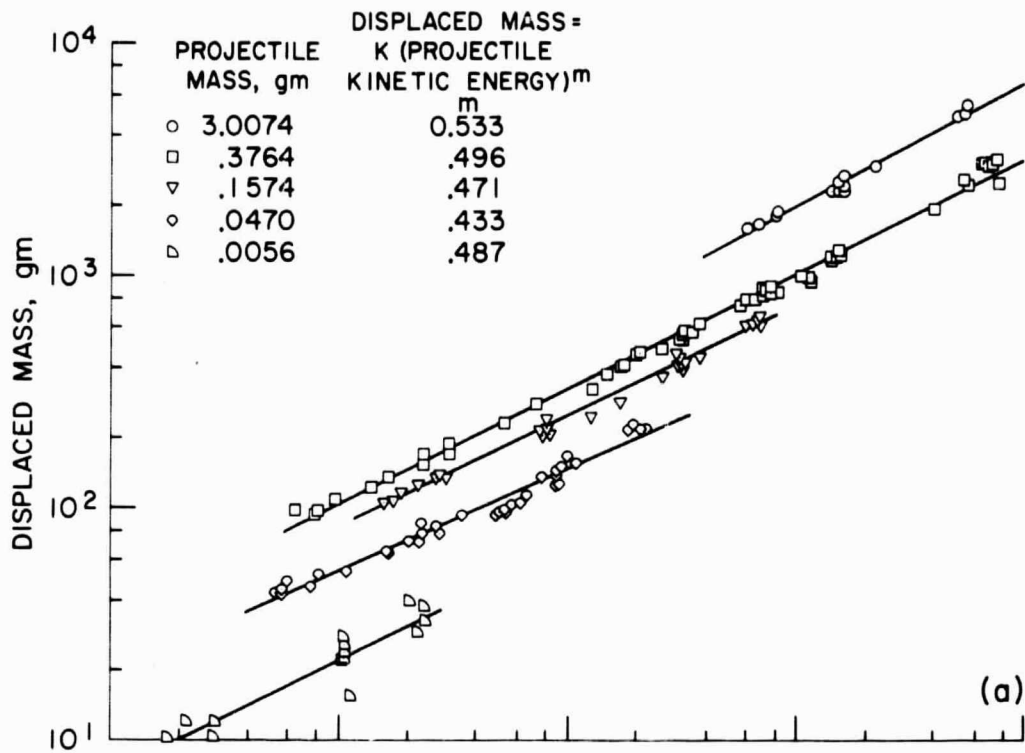
Figure 1

Figure 2

Figure 3.

M.D.O.B. =

0mm ± 1mm

3.2 mm ± 1mm

6.3 mm ± 1mm

9.5mm ± 1mm

14.3 mm ± 1mm

−35　　　0　　　+35
cm

Figure 4, page 1

M.D.O.B.:

27.0 mm ± 1 mm

39.7 mm ± 1 mm

52.5 mm ± 1 mm

65.2 mm ± 1 mm
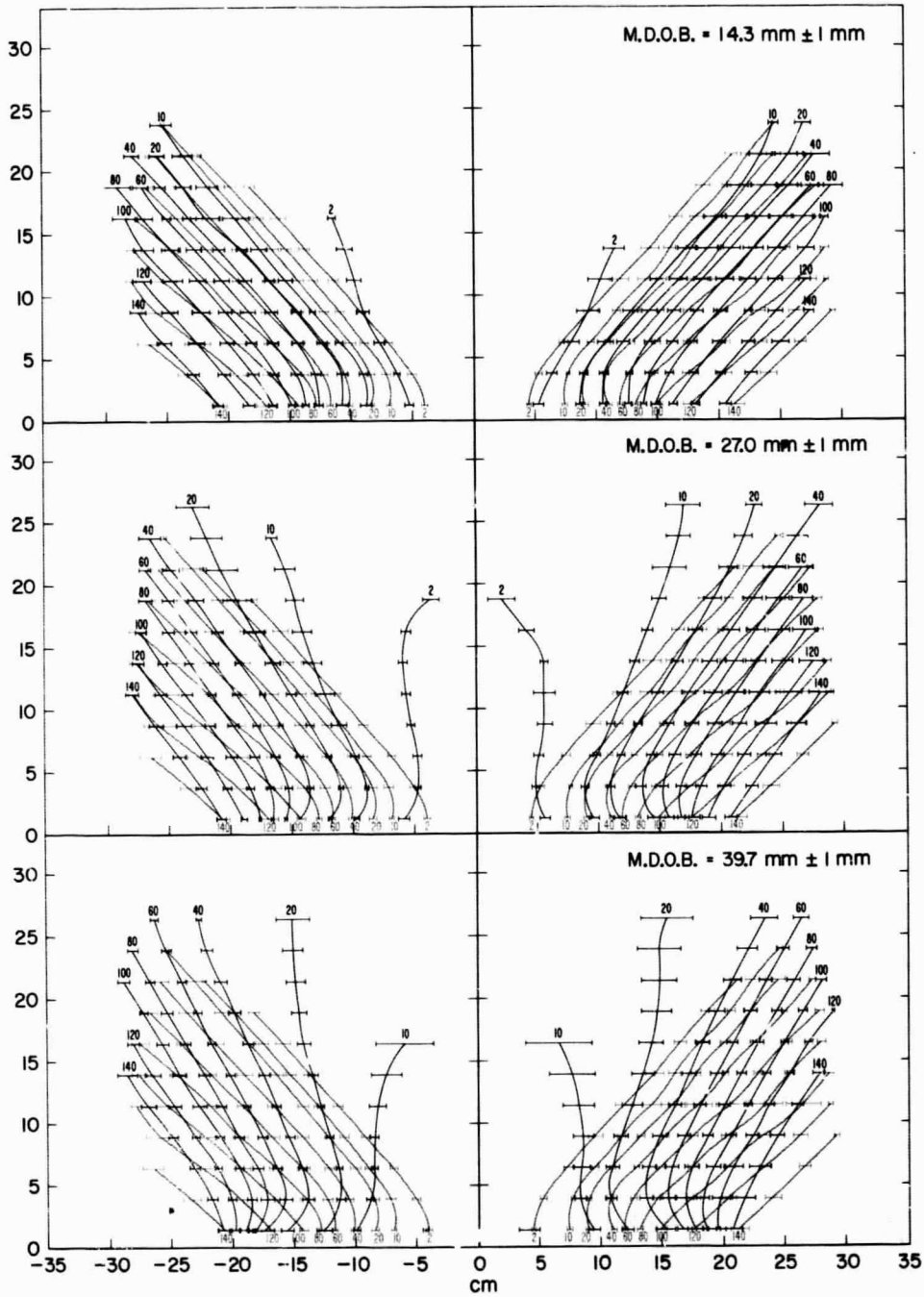
77.8 mm ± 1 mm

−35

0
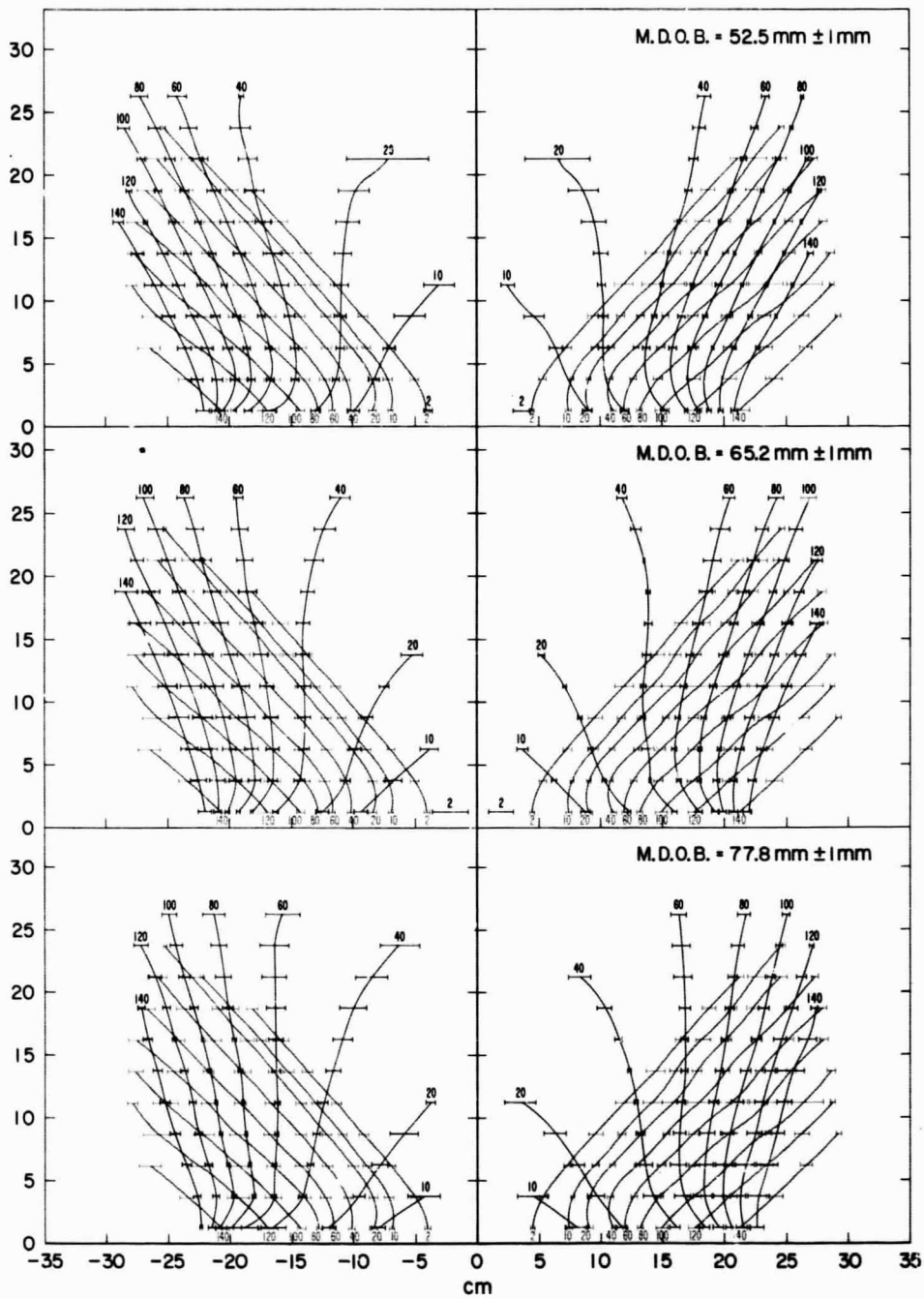cm

+35
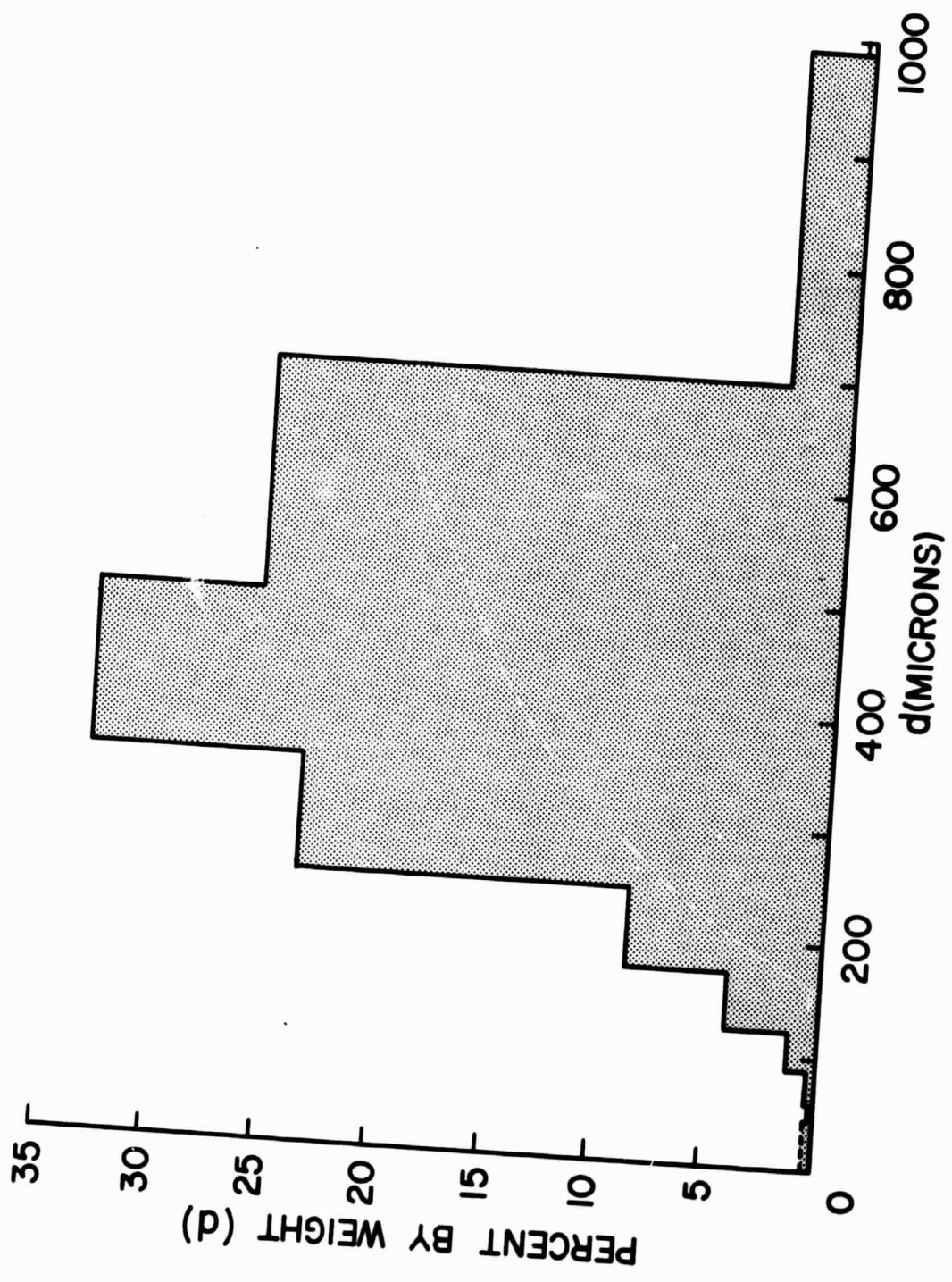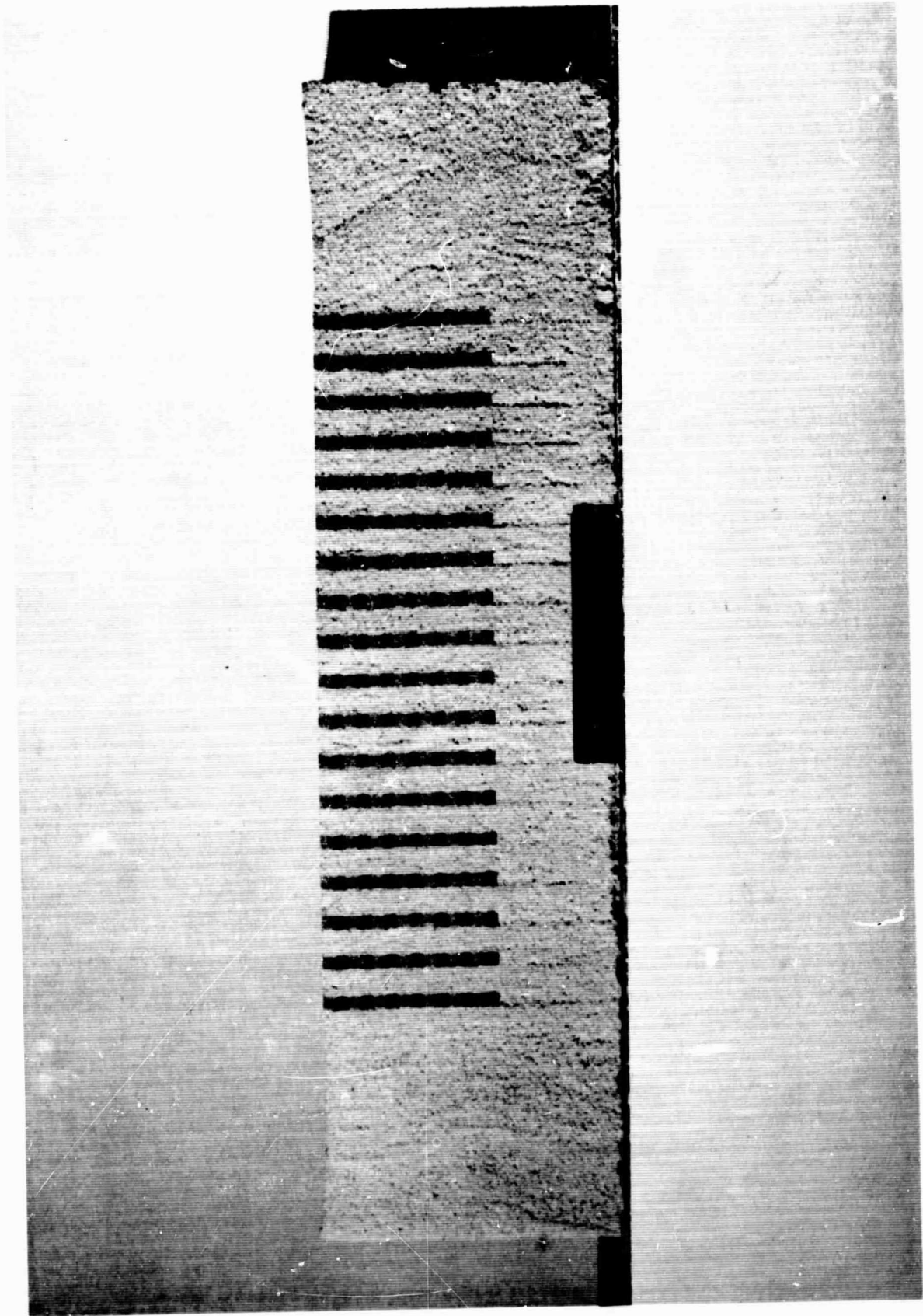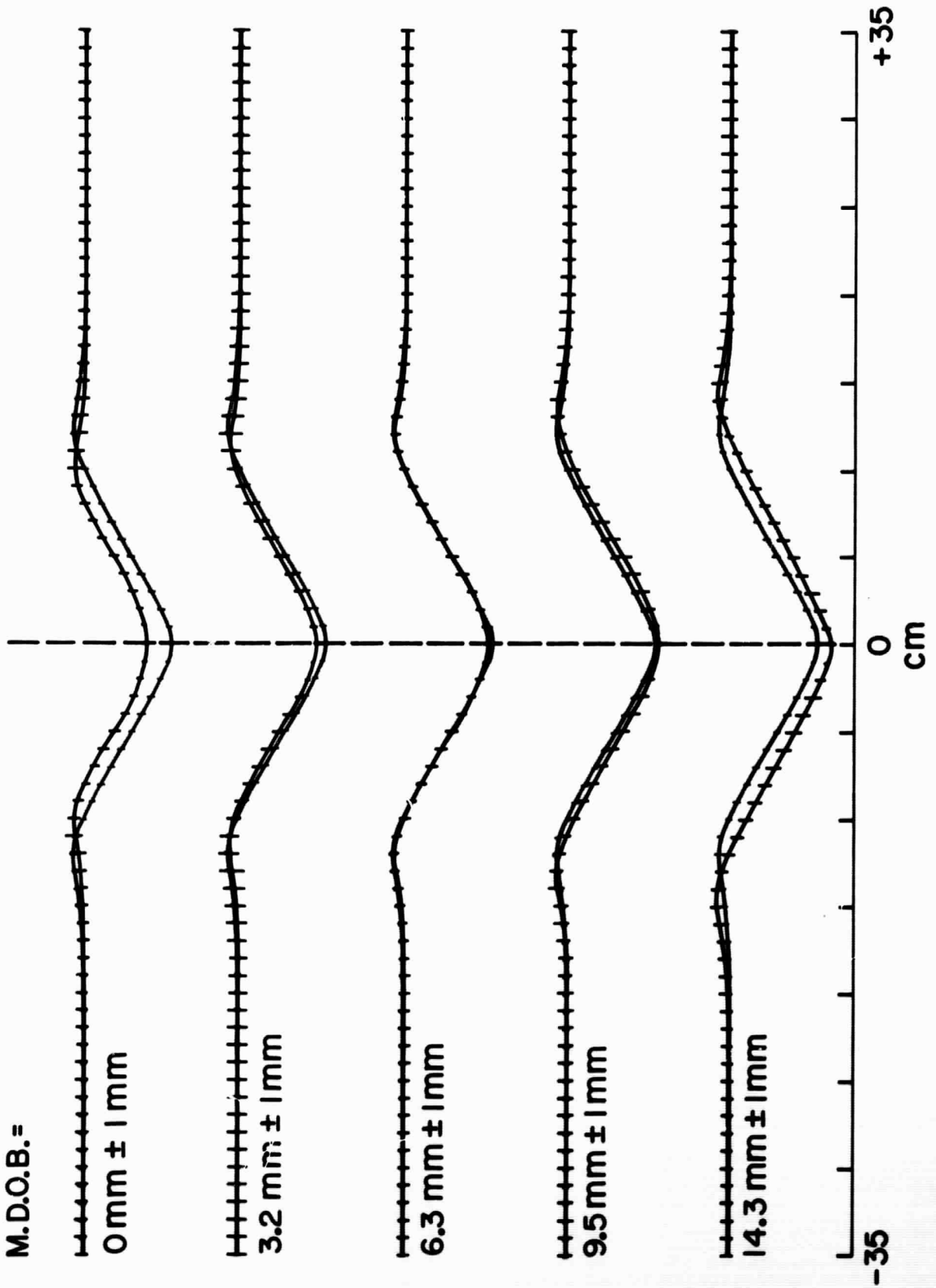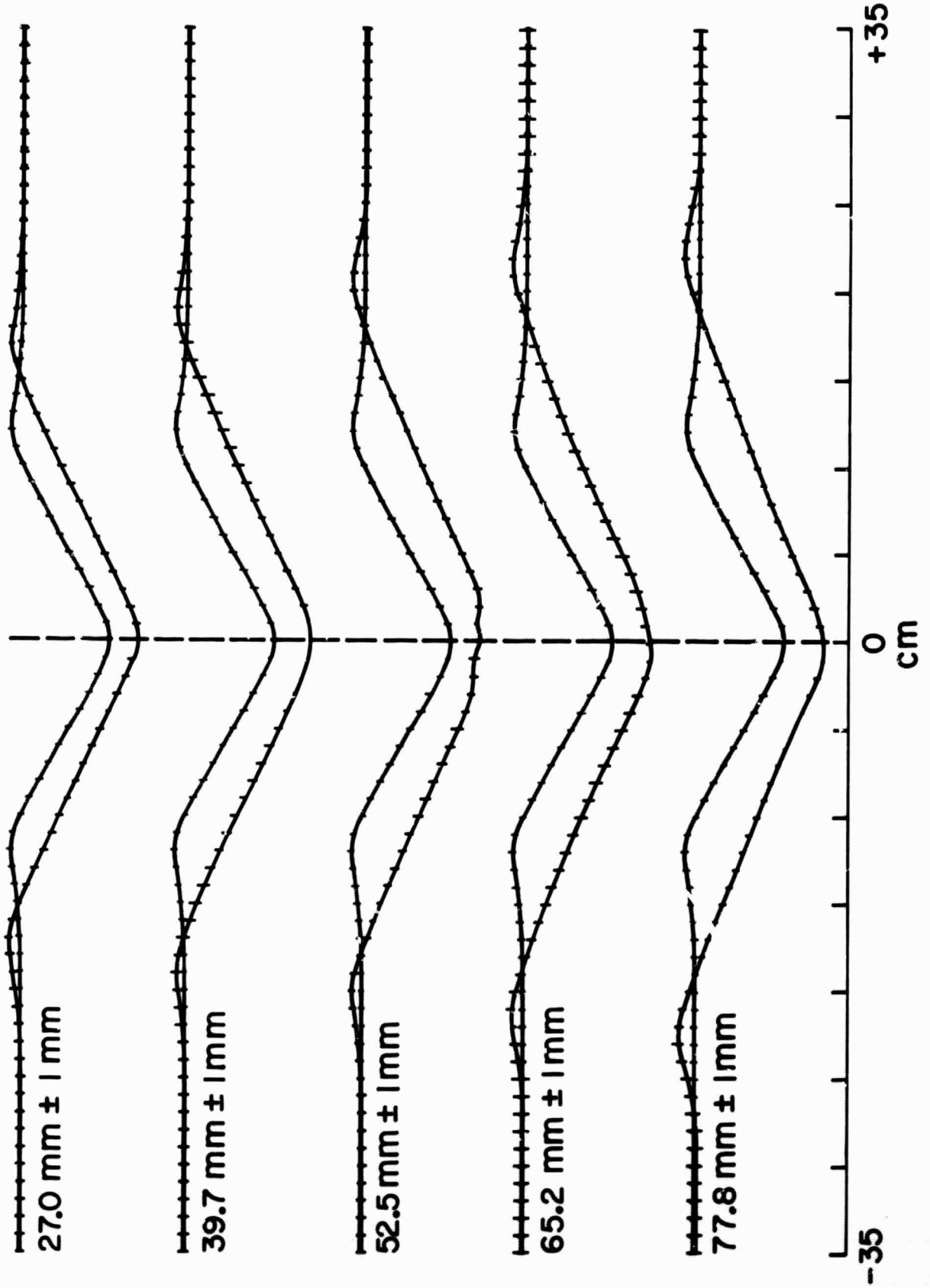
Figure 4, page 2
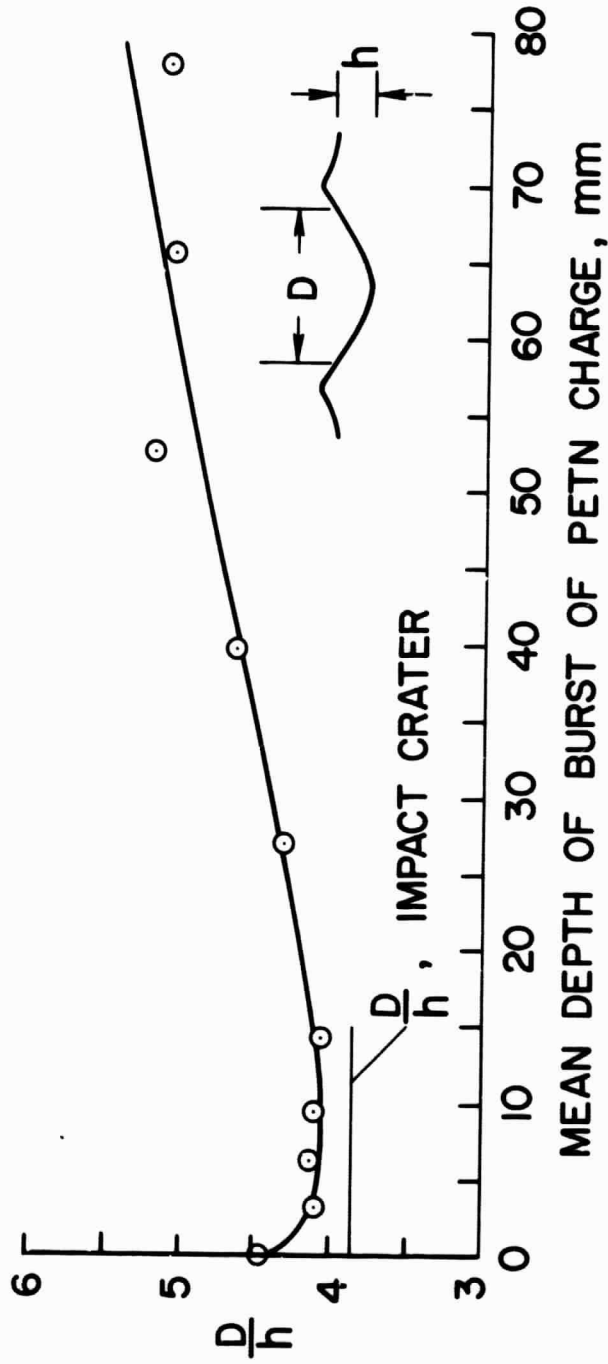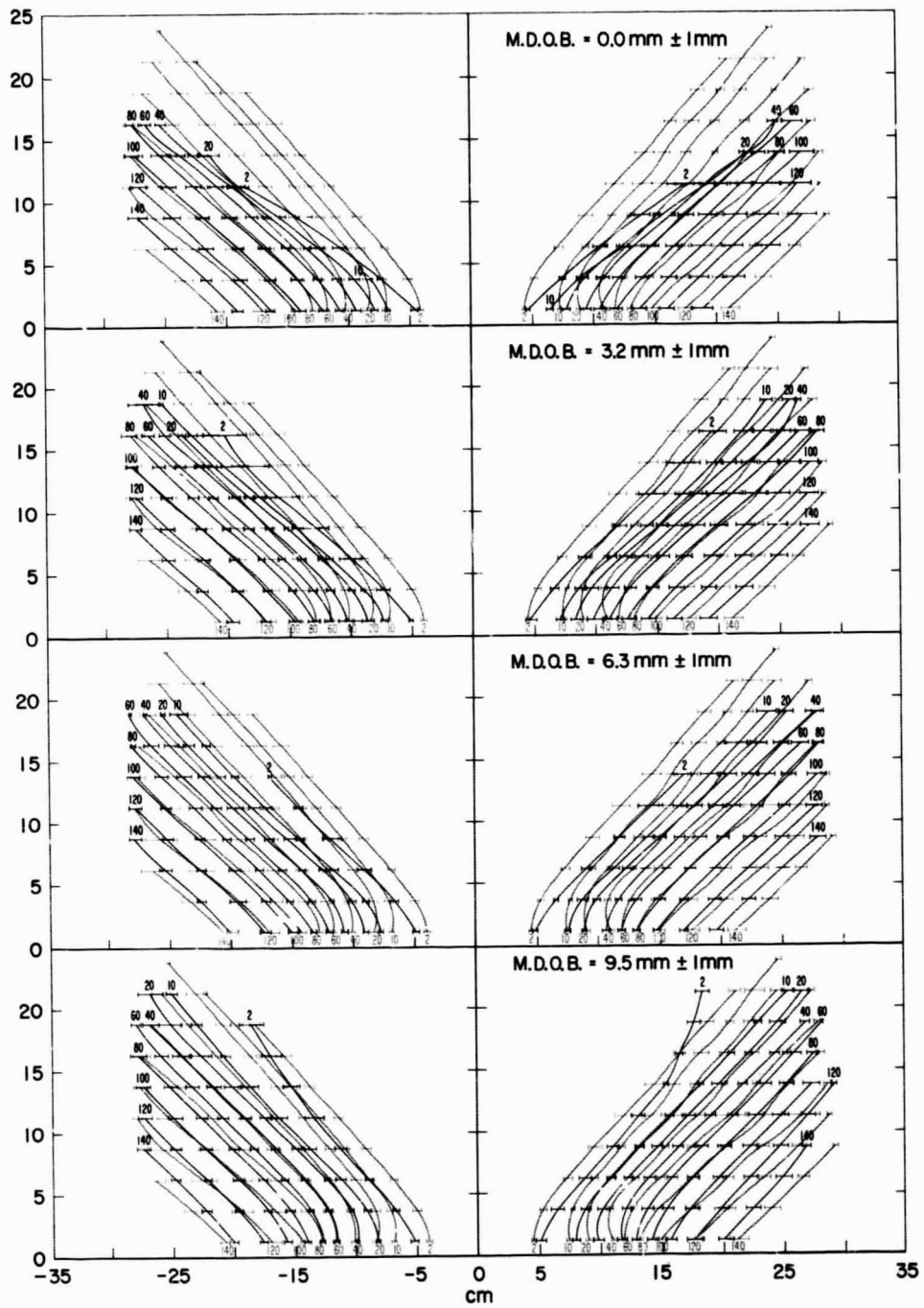
Figure 5

Figure 6, page 1

Figure 6, page 2

Figure 6 , page 3

Figure 7
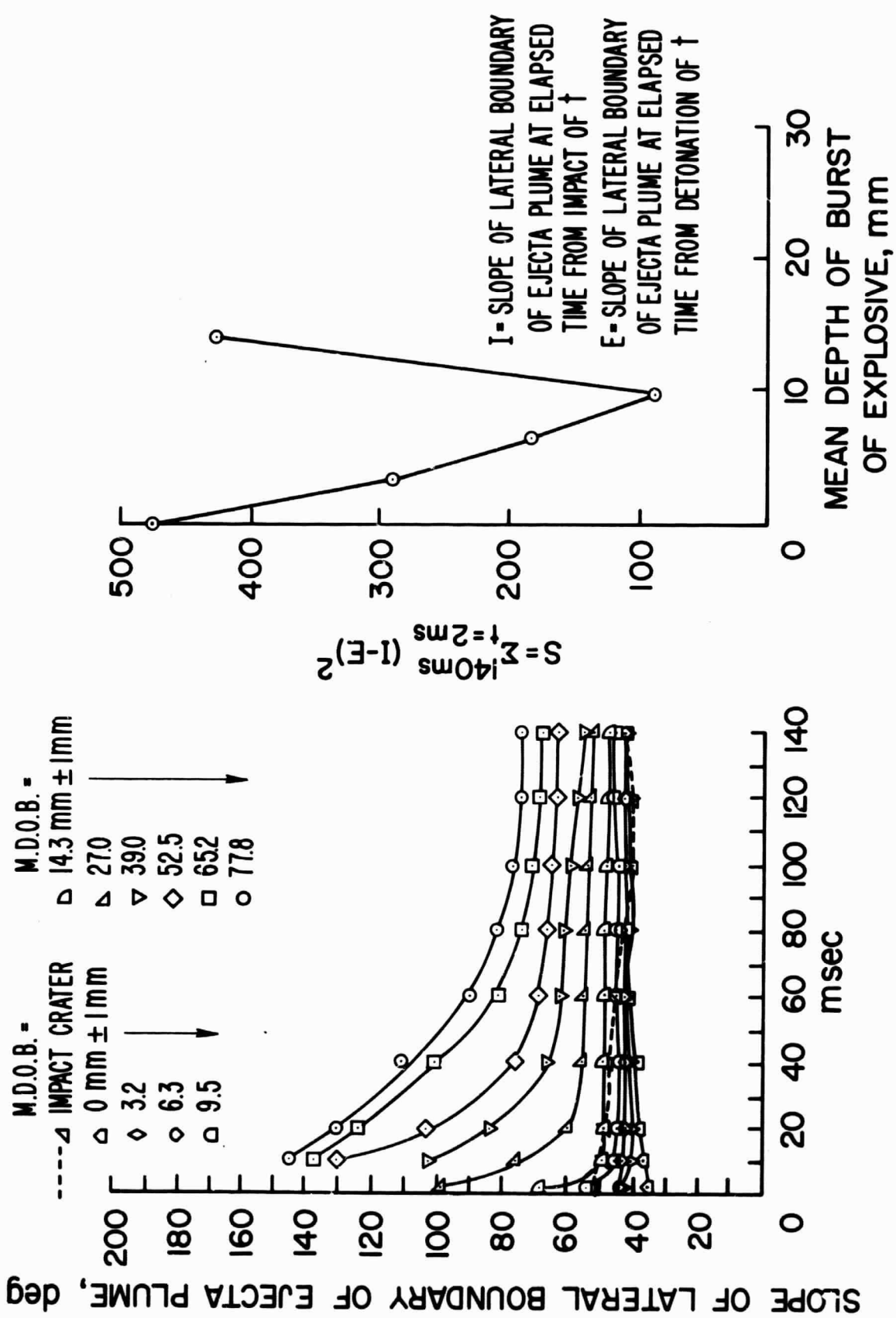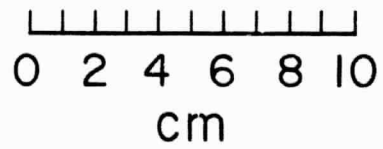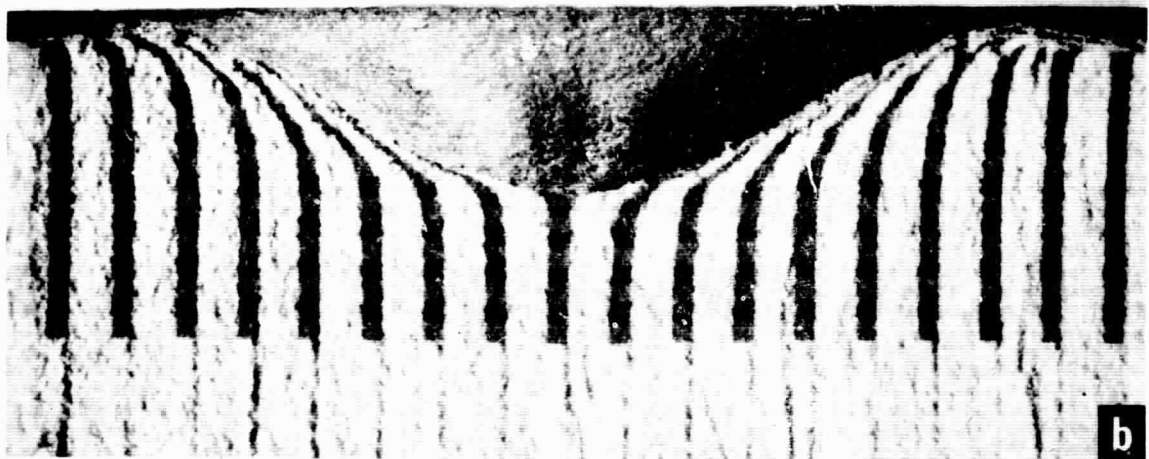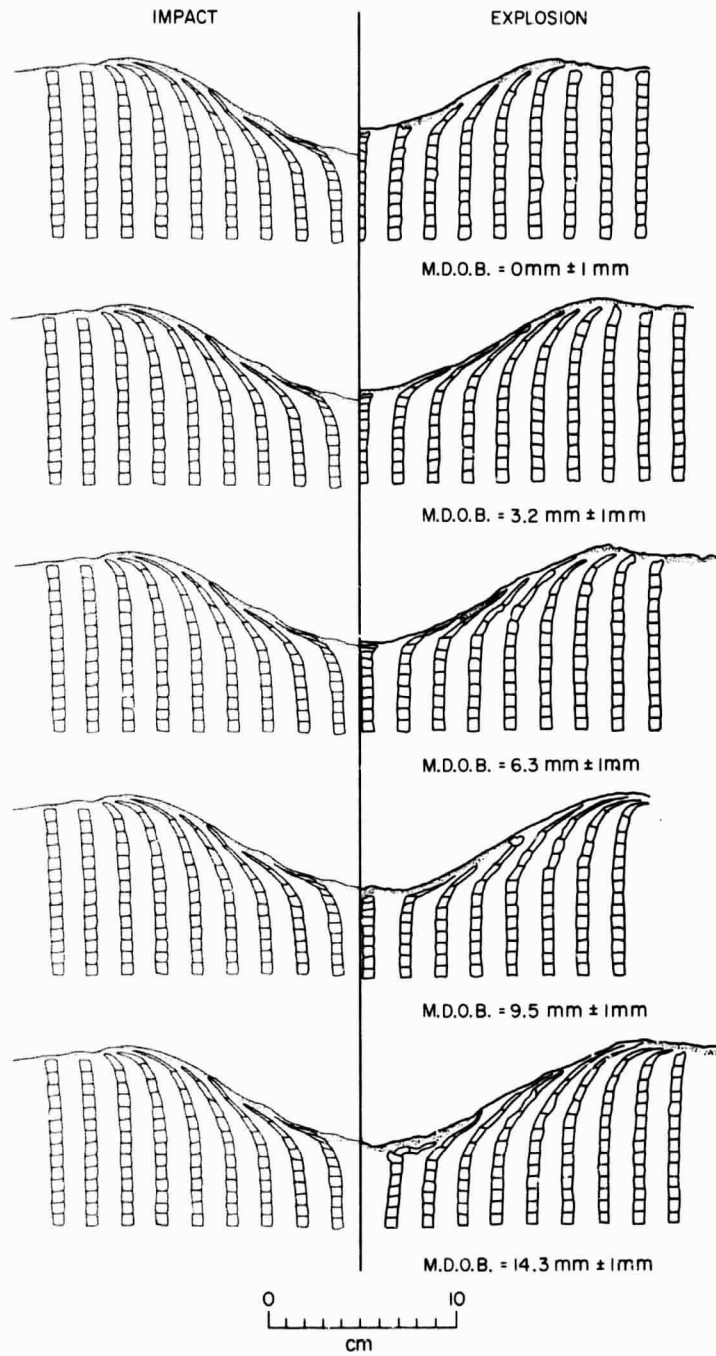
Figure 8.

IMPACT EXPLOSION

M.D.O.B. = 0mm ± 1mm

M.D.O.B. = 3.2 mm ± 1mm

M.D.O.B. = 6.3 mm ± 1mm

M.D.O.B. = 9.5 mm ± 1mm

M.D.O.B. = 14.3 mm ± 1mm

0   10
cm

Figure 9, page 1

IMPACT   EXPLOSION

M.D.O.B. = 27.0 mm ± 1mm

M.D.O.B. = 39.7 mm ± 1mm
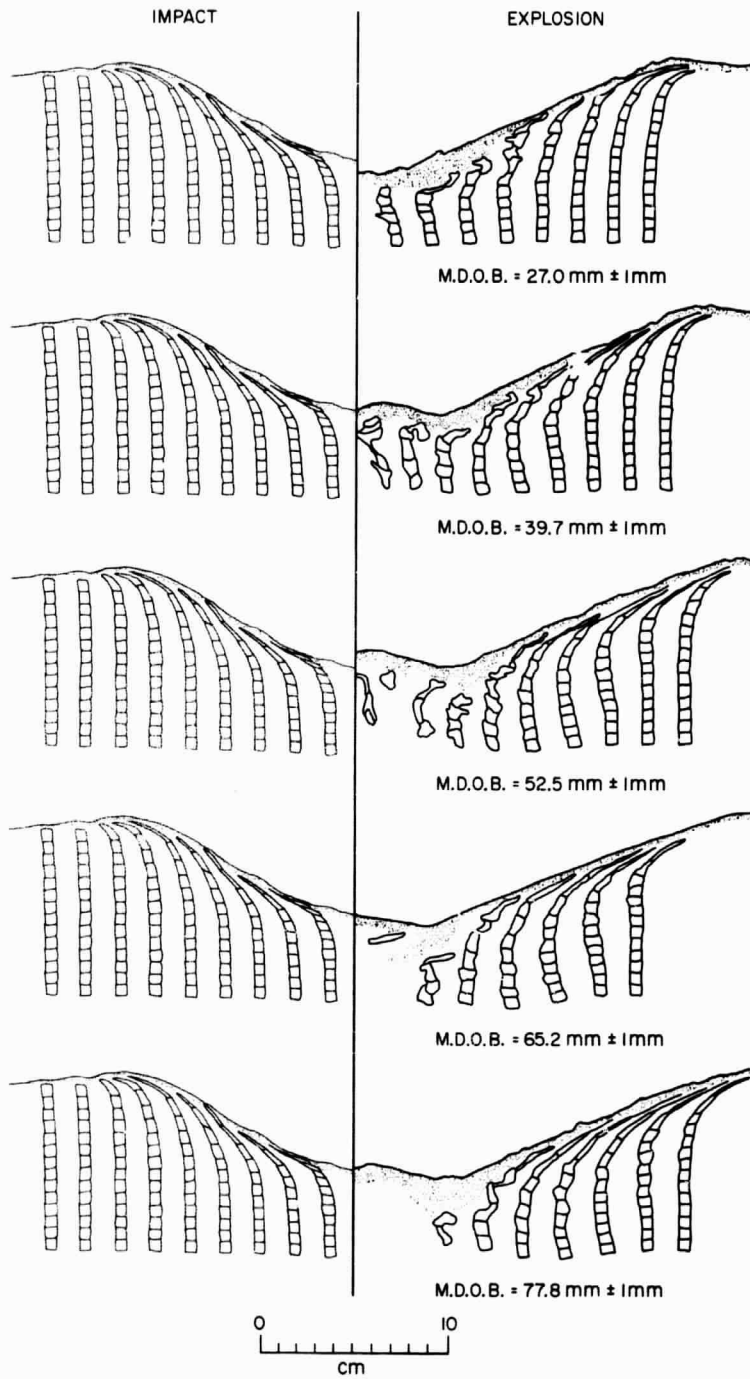
M.D.O.B. = 52.5 mm ± 1mm

M.D.O.B. = 65.2 mm ± 1mm

M.D.O.B. = 77.8 mm ± 1mm

0   10
cm

Figure 9, page 2

Figure 10.